J. Fluid Mech. (2007), *vol.* 589, *pp.* 157–181.
doi:10.1017/S0022112007007586 Printed in the United Kingdom

Motion of a capsule in a cylindrical tube: effect of membrane pre-stress

YANNICK LEFEBVRE AND DOMINIQUE BARTHÈS-BIESEL

UMR CNRS 6600, Biomécanique et Génie Biomédical, Université de Technologie de Compiègne, France

(Received 20 July 2006 and in revised form 16 May 2007)

We present a numerical model of the axisymmetric flow of an initially spherical capsule in a co-axial cylindrical tube. The capsule consists of a liquid droplet enclosed by a thin hyper-elastic membrane that is assumed to obey different membrane constitutive equations such as Mooney–Rivlin, Skalak *et al.* (1973) or Evans & Skalak (1980) laws. It is further assumed that the capsule may be subjected to some isotropic pre-stress due to initial swelling. We compute the steady flow of the capsule inside the tube as a function of the size ratio between the capsule and tube radii, the amount of pre-swelling and the membrane constitutive law. We thus determine the deformed profile geometry and specifically the onset of the curvature inversion at the back of the particle. We show that for a given size ratio, the critical flow rate at which the back curvature changes is strongly dependent on pre-inflation. The elastic tension level in the membrane as well as the additional pressure drop created by the presence of the particle are also computed. The numerical results are then compared to experimental observations of capsules with alginate membranes as they flow in small tubes (Risso *et al.* 2006). It is found that the experimental capsules were probably pre-inflated by about 3% and that their membrane is best modelled by the Skalak *et al.* law.

1. Introduction

A simple capsule consists of a liquid droplet surrounded by a thin membrane that controls exchanges between the environment and the capsule's internal contents and has thus a protection role. Such particles may be considered as models of simple cells such as red blood cells, but they are also found in many industrial applications where a substance has to be protected until ready to be used. For example, there are capsules in a number of common products such as pesticides, inks, and cosmetics. They are also used for bioengineering applications like drug targeting or cell encapsulation (Kühtreiber, Lanza & Chick 1998). In most situations, capsules are suspended in another liquid and are thus subjected to hydrodynamic forces when the suspension is flowing. The motion of the suspending and internal liquids creates a viscous deformation and may lead to breakup. The control of this process is essential for the design of artificial capsules and a number of studies have been published over the years on this topic.

Most models consider the simple prototypical case of a capsule consisting of a Newtonian incompressible liquid droplet surrounded by an infinitely thin membrane that can be treated as a two-dimensional elastic surface with known mechanical properties. Thus, the deformation of an initially spherical capsule freely suspended in a shear flow has been computed as a function of shear rate when the membrane obeys

a neo-Hookean type of law (e.g. Li, Barthès-Biesel & Helmy 1988; Ramanujan & Pozrikidis 1998; Eggleton & Popel 1998; Diaz, Pelekasis & Barthès-Biesel 2000; Lac *et al.* 2004). Area-incompressible membranes have been considered to model the behaviour of red blood cells or lipid vesicles (e.g. Kraus *et al.* 1996; Ramanujan & Pozrikidis 1998; Eggleton & Popel 1998). The bending rigidity of the membrane has also been taken into account (Kraus *et al.* 1996; Kwak & Pozrikidis 1998). Lac *et al.* (2004) compared different membrane laws where the shear and area dilation modulus were of the same order of magnitude. They find that the elastic constitutive law of the membrane significantly affects the overall deformation of a capsule subjected to an unbounded shear flow. In particular, they show that at shear rates lower than some critical value, the capsule reaches an equilibrium deformed state that is unstable owing to the presence of negative principal tensions that cause membrane buckling. They also find that for shear rates larger than another critical value, no equilibrium can be obtained and breakup would be assumed to occur. All the above studies assume that the initial capsule shape is unstressed.

Another situation of interest that has not been studied much is where the external flow is bounded. This occurs when the capsule is forced to flow into a small pore with cross-section dimensions of the same order as its own. This configuration is found in blood microcirculation, in filtration or in transport of a capsule suspension in microchannels. For example, the flow of red blood cells in microvessels has been modelled for centred or off-centred cells (Secomb 1995). Then the 'capsule' is not initially spherical (discocyte shape) and its deformation is strongly dependent on the membrane being area incompressible. The case of initially spherical capsules enclosed by a neo-Hookean membrane flowing through cylindrical pores has been considered by Quéguiner & Barthès-Biesel (1997) who showed that the capsule takes a steady parachute shape when its radius is smaller than or equal to the pore radius. When its radius is larger than the pore's, the capsule takes a slug shape. These results have been completed by Diaz & Barthès-Biesel (2002) who considered different constitutive laws for the membrane and different initial capsule geometries, as measured by a sphericity index. They showed that, at high flow strength, the membrane constitutive law and the surface to volume ratio have a measurable influence on the geometry of the final deformed parachute shape and on the additional pressure drop created by the capsule. They also studied the influence of the viscosity ratio between the internal and external liquids on the transient entrance phase and showed that increasing the capsule internal viscosity led to larger pressure peaks during entrance. The case of an axisymmetric file of red blood cells has also been considered by Pozrikidis (2005), who studied the influence of the cell to vessel radius ratio and of cell spacing on the dynamics of the suspension.

Recently, Risso, Collé-Paillot & Zagzoule (2006) reported a thorough experimental study of the flow in a cylindrical pore of initially spherical capsules with a membrane made of alginate covalently linked to human serum albumin (HSA). The capsule membrane elastic properties were measured by means of compression experiments (Carin *et al.* 2003; Risso & Carin 2004) and the steady capsule profile in the tube was recorded with a video camera as a function of flow strength and size ratio between the capsule and the tube. A comparison of the experimental profiles and those predicted by Quéguiner & Barthès-Biesel (1997) showed that the agreement was not very good, and that the numerical deformation was larger than the measured one.

However, a previous experimental study of the same capsules (Sherwood *et al.* 2003) had shown that they were prone to osmotic effects owing to the presence of large polyelectrolytes in the internal liquid due to partial dissolution of the membrane material.

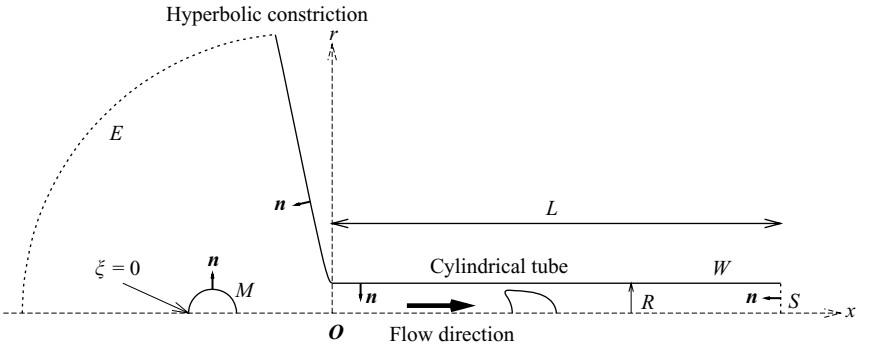

FIGURE 1. Capsule flowing into a channel consisting of an hyperbolic entrance followed by a cylindrical tube.

Thus one is led to suspect that in Risso *et al.*'s (2006) experiments, the capsules may have been subjected to internal pre-stress due to uncontrolled osmotic phenomena. Such pre-stress can have a significant effect on the deformation of capsules subjected to flow as was recently reported by Lac & Barthès-Biesel (2005) in the case of an unbounded simple shear flow. In particular, they showed that pre-stress could remove the membrane buckling instability observed for low flow strength (Lac *et al.* 2004) and that it lowered the capsule deformation for a given shear rate.

Since membrane pre-stress is important in determining the motion of capsules in unbounded shear flow, it should be equally important for pore flow. This paper thus presents a study of the effect of pre-stress on the motion of an initially spherical capsule in a cylindrical pore. We first consider the case where the capsule membrane satisfies the Skalak *et al.* (1973) constitutive law with comparable values of the shear and area dilation modulus, and study the influence of flow strength, membrane pre-stress and size ratio between the capsule and the tube on the steady deformed state of the capsule. We then compare the numerical shapes to those measured by Risso *et al.* (2006) and show the existence of a probable pre-swelling of the experimental capsules. Other membrane constitutive laws are then considered and we show that the best fit with experiments is obtained with the Skalak *et al.* (1973) law when large deformations are achieved.

2. Problem statement

2.1. *Flow problem*

The flow situation is identical to the one studied by Quéguiner & Barthès-Biesel (1997) and by Diaz & Barthès-Biesel (2002) and will be only summarised in the following. We consider an axisymmetric situation where the channel and the capsule have the same axis of revolution Ox. The channel consists of an axisymmetric hyperbolic entrance extended at the hyperboloid apex by a cylindrical part (denoted 'tube') of radius R and axis Ox, where O is located at the beginning of the cylinder (figure 1). The opening of the entrance (defined by the angle between Ox and the hyperbola asymptote) has no influence on the steady capsule motion in the cylindrical part and only determines the transient flow of the particle into the tube. The channel is filled with an incompressible Newtonian liquid of viscosity $\mu^{(1)}$ flowing with flow rate Q. The flow Reynolds number is assumed to be very small and the axisymmetric velocity field in the absence of a particle is denoted $\boldsymbol{v}^{\infty}$. The capsule is initially spherical

with radius a. It is filled with a Newtonian incompressible liquid with viscosity $\mu^{(2)}$ and enclosed by an infinitely thin hyperelastic membrane with surface shear elastic modulus G_s and area dilation modulus K_s. Buoyancy forces are neglected and consequently, when the capsule is centred on Ox, it takes an axisymmetric deformed shape and remains centred. The position of the capsule centre of mass on Ox is denoted $\boldsymbol{x}^{(M)} = x^{(M)}\boldsymbol{e}_x$ where $\boldsymbol{e}_x$ is the axis unit vector. The unit normal vector $\boldsymbol{n}$ to all the boundaries points into the suspending liquid.

The internal and external liquid motion satisfies the Stokes equations:

$$\nabla \cdot \boldsymbol{\sigma}^{(\beta)} = \boldsymbol{0}, \quad \nabla \cdot \boldsymbol{v}^{(\beta)} = 0, \tag{2.1}$$

$$\boldsymbol{\sigma}^{(\beta)} = -p^{(\beta)}\boldsymbol{I} + \mu^{(\beta)}\left(\nabla \boldsymbol{v}^{(\beta)} + \left(\nabla \boldsymbol{v}^{(\beta)}\right)^T\right), \tag{2.2}$$

where $\boldsymbol{v}^{(\beta)}$, $\boldsymbol{\sigma}^{(\beta)}$ and $p^{(\beta)}$ denote the velocity, stress and pressure fields in the suspending ($\beta = 1$) and internal ($\beta = 2$) liquids.

The associated boundary conditions are:
no flow disturbance far from the capsule

$$\boldsymbol{v}^{(1)}(\boldsymbol{x}, t) \to \boldsymbol{v}^{\infty}(\boldsymbol{x}), \quad \left|\boldsymbol{x} - \boldsymbol{x}^{(M)}\right| \gg R; \tag{2.3}$$

no slip on the channel wall (W)

$$\boldsymbol{v}^{(1)}(\boldsymbol{x}, t) = \boldsymbol{0}, \quad \boldsymbol{x} \in W; \tag{2.4}$$

no slip on the capsule deformed surface (M)

$$\boldsymbol{v}^{(1)}(\boldsymbol{x}, t) = \boldsymbol{v}^{(2)}(\boldsymbol{x}, t) = \frac{\partial}{\partial t}\boldsymbol{x}(\boldsymbol{X}, t), \quad \boldsymbol{x} \in M, \tag{2.5}$$

where $\boldsymbol{X}$ denotes the initial position of a membrane material point located at position $\boldsymbol{x}$ at time t;
the load $\Delta \boldsymbol{f}$ on the membrane is due to the viscous traction jump

$$\left(\boldsymbol{\sigma}^{(1)} - \boldsymbol{\sigma}^{(2)}\right) \cdot \boldsymbol{n} + \Delta \boldsymbol{f} = \boldsymbol{0}, \quad \boldsymbol{x} \in M, \tag{2.6}$$

where $\boldsymbol{n}$ is the outer unit normal vector to M.

2.2. *Capsule membrane mechanics*

It remains to relate the load $\Delta \boldsymbol{f}$ to the capsule deformation. A detailed discussion of membrane mechanics is given by Pozrikidis (2003*a*, *b*), or by Barthès-Biesel, Diaz & Dhenin (2002) and Barthès-Biesel (2003). We assume that the membrane is made of an infinitely thin sheet of a hyperelastic material with in-plane isotropy.

2.2.1. *Membrane deformation*

Then, under axisymmetric load conditions, the deformation and elastic tension tensors are both axisymmetric with common principal directions along the meridian (index 1) and parallel (index 2) curves. We use cylindrical coordinates (x, r) and define the deformed position of a membrane material point by (s, r) (respectively (ξ, ρ) in the initial state), where s (respectively ξ) is the arc length measured along a meridian curve with $s = 0$ (respectively $\xi = 0$) at the downstream intersection of the meridian with Ox (figure 1). The principal elongation ratios λ_1 and λ_2 are given by

$$\lambda_1 = \frac{\mathrm{d}s}{\mathrm{d}\xi}, \quad \lambda_2 = \frac{r}{\rho}, \tag{2.7}$$

and the principal curvatures C_1 and C_2 by

$$C_1 = -\frac{\mathrm{d}\boldsymbol{\tau}}{\mathrm{d}s}\cdot\boldsymbol{n}, \quad C_2 = \frac{n_r}{r}, \tag{2.8}$$

where $\boldsymbol{\tau}$ is the unit tangent vector to the meridian oriented along increasing s and n_r is the radial component of $\boldsymbol{n}$.

2.2.2. *Membrane constitutive law*

The membrane constitutive law relates the tensions to the deformations. A number of laws have been proposed to model thin membranes, but we consider only the simplest ones with constant material coefficients. One candidate is the Mooney–Rivlin law (MR) that models an infinitely thin sheet of a three-dimensional isotropic volume-incompressible material:

$$T_1 = \frac{G_s}{\lambda_1\lambda_2}\left[\lambda_1^2 - \frac{1}{(\lambda_1\lambda_2)^2}\right]\left[\Psi + \lambda_2^2(1-\Psi)\right], \tag{2.9}$$

where the parameter Ψ varies between 0 and 1. The value $\Psi = 1$ corresponds to a neo-Hookean material, while $\Psi = 0$ corresponds to the so-called extreme Mooney–Rivlin material. The area dilation modulus K_s is then equal to $3G_s$ (Barthès-Biesel *et al.* 2002).

Another approach consists of treating the membrane as a two-dimensional continuum with in-plane isotropy. Correspondingly, starting from general principles of elasticity and thermodynamics, Skalak *et al.* (1973) derived the following law (Sk):

$$T_1 = \frac{G_s}{\lambda_1\lambda_2}\left[\lambda_1^2\left(\lambda_1^2 - 1\right) + C(\lambda_1\lambda_2)^2[(\lambda_1\lambda_2)^2 - 1]\right], \tag{2.10}$$

where the relation between the surface shear elastic modulus G_s and the area dilation modulus K_s depends on the dimensionless parameter C:

$$K_s = G_s(1 + 2C). \tag{2.11}$$

This law was later simplified by Evans & Skalak (1980) (ES) who proposed adding linearly and independently the contributions of shear and area dilation:

$$T_1 = G_s\left[\frac{1}{2\lambda_1^2\lambda_2^2}\left(\lambda_1^2 - \lambda_2^2\right) + A(\lambda_1\lambda_2 - 1)\right], \tag{2.12}$$

where the area dilation modulus is simply proportional to the shear modulus:

$$K_s = AG_s. \tag{2.13}$$

In all three laws, the expression for T_2 is obtained by interchanging the roles of indices 1 and 2.

The Sk and ES laws were initially designed to model the area-incompressible membrane of biological cells such as red blood cells, corresponding to $C \gg 1$ or $A \gg 1$. However, those laws are very general and can also be used to model other types of membranes for which K_s and G_s are of the same order of magnitude, as is the case for alginate membranes (Carin *et al.* 2003).

When $C = 1$ and $A = 3$, the MR, Sk and ES laws predict the same small deformation of the membrane with $K_s = 3G_s$. However, they lead to different nonlinear tension–strain relations under large deformations. In particular, it is easily checked that the MR and ES laws are strain-softening under uniaxial stretching ($T_1 \neq 0$, $T_2 = 0$), whereas the Sk law is strain-hardening (Barthès-Biesel *et al.* 2002). These three laws

(2.9), (2.10), (2.12) have been used to analyse compression experiments performed on capsules with alginate membranes (Carin *et al.* 2003). The technique consists of placing a capsule between two parallel plates and measuring simultaneously the distance between the plates and the applied force. Large reversible elastic deformations are achieved, and the membrane elastic parameters are obtained by means of an inverse analysis of the compression experiment. It is found that for freshly prepared capsules with thin membranes (with thickness less than 5% of the radius), the MR law with $\Psi = 0$ or Sk and ES laws with $K_s = G_s$ could all be used to fit the experimental compression data with good precision, whereas the commonly used neo-Hookean law (i.e. MR with $\Psi = 1$) could not (Carin *et al.* 2003; Risso & Carin 2004; Rachik *et al.* 2006). However, for capsules that had been stored for over six months in saline solution, Risso & Carin (2004) find that the ES law gives better fit with the data than the Sk or MR laws.

It is clear that a single experiment, such as compression between plates, is not sufficient to determine unambiguously the constitutive law for the membrane. It will thus be of interest to apply a similar inverse analysis to the flow of a capsule in a tube, and try to deduce a membrane constitutive law from the analysis of the capsule motion and deformation as a function of flow strength.

2.2.3. *Membrane equilibrium equations*

Diaz & Barthès-Biesel (2002) observed a tendency towards buckling of the downstream part of the membrane under certain flow conditions, particularly during the entrance phase into the tube. To solve this problem, they assumed that the membrane had a small bending rigidity and that the principal bending moments m_1 and m_2 depended linearly on the local curvature change (Pozrikidis 2003*b*):

$$m_1 = \frac{B_s}{\lambda_2}\left[\lambda_1 C_1 - C_1^0 + \nu_s\left(\lambda_2 C_2 - C_2^0\right)\right], \tag{2.14}$$

where B_s is the bending modulus, C_1^0 and C_2^0 are the principal initial curvatures and where ν_s depends on the membrane constitutive law and is equal to $1/2$, $C/(C+1)$ or $(A-1)/(A+1)$ for the MR, Sk or ES laws, respectively. The expression for m_2 is obtained by interchanging indices 1 and 2. The axisymmetric membrane equilibrium equations are then given by:

$$\Delta \boldsymbol{f} \cdot \boldsymbol{\tau} = \frac{\mathrm{d}T_1}{\mathrm{d}s} + \frac{1}{r}\frac{\mathrm{d}r}{\mathrm{d}s}(T_1 - T_2) - C_1\left[\frac{1}{r}\frac{\mathrm{d}r}{\mathrm{d}s}m_2 - \frac{1}{r}\frac{\mathrm{d}}{\mathrm{d}s}(rm_1)\right], \tag{2.15}$$

$$\Delta \boldsymbol{f} \cdot \boldsymbol{n} = -C_1 T_1 - C_2 T_2 - \frac{1}{r}\frac{\mathrm{d}}{\mathrm{d}s}\left[\frac{\mathrm{d}r}{\mathrm{d}s}m_2 - \frac{\mathrm{d}}{\mathrm{d}s}(rm_1)\right], \tag{2.16}$$

where $\Delta \boldsymbol{f}$ is the viscous traction jump defined in (2.6).

2.2.4. *Pre-stress*

Following Lac & Barthès-Biesel (2005), we further assume that the capsule is subjected to a positive osmotic pressure difference $p^{(0)}$ between the internal and external phases. Consequently, since the capsule is spherical, the membrane is pre-stressed by an isotropic elastic tension $T^{(0)}$ given by the Laplace law:

$$T_1 = T_2 = T^{(0)} = \frac{ap^{(0)}}{2}, \tag{2.17}$$

where a is the radius of the inflated capsule. The membrane is thus stretched with an initial elongation $\lambda^{(0)}$:

$$\lambda_1 = \lambda_2 = \lambda^{(0)} = \frac{a}{a_0} = 1 + \alpha, \tag{2.18}$$

where a_0 is the capsule radius in the unstressed configuration. As shown by Lac & Barthès-Biesel (2005), the relation between $T^{(0)}$ and α depends on the membrane constitutive law (and thus on C, A or Ψ). However it is independent of bending resistance since bending moments are identically zero for isotropic swelling.

2.3. *Boundary integral formulation*

The boundary integral form of the Stokes equations is used. As shown in figure 1, the external flow domain is bounded by the capsule membrane M, the channel wall W, a spherical entrance surface E centred on O with radius R_E ($R_E \gg R$), a planar exit section S normal to Ox and located far inside the pore at $x = L$ ($L \gg R$). The internal flow domain is bounded by M. At time $t = 0$, the initially spherical, pre-inflated or not, capsule is centred at $x^{(M)}(0) = -d$ ($0 < d \ll R_E$) and flow is started with constant flow rate Q. We then follow the motion of the capsule inside the pore, making sure that at all times $x^{(M)} \ll L$. We take the entrance pressure as reference ($p = 0$ on E). Then, there is no contribution to the boundary integral from terms evaluated on E where the velocity is $O(Q/R_E^2)$. On the exit surface S, Poiseuille flow conditions prevail:

$$\boldsymbol{v}^{(1)}(\boldsymbol{x}, t) = \boldsymbol{v}^{\infty}(\boldsymbol{x}) = 2\frac{Q}{\pi R^2}\left[1 - \left(\frac{r}{R}\right)^2\right]\boldsymbol{e}_x, \quad p = p^{\infty}(L) + \Delta p, \tag{2.19}$$

where Δp is the additional pressure drop created by the capsule and $p^{\infty}(L)$ is the pressure that would exist in the absence of a particle.

The effect of the viscosity ratio $\mu^{(2)}/\mu^{(1)}$ between the internal and external liquids on the transient entrance flow has been studied by Diaz & Barthès-Biesel (2002). Here we concentrate on the steady motion of the capsule inside the tube. When such a steady state is reached, the internal liquid is at rest and its viscosity $\mu^{(2)}$ has no influence on capsule motion and deformation. Consequently, we choose $\mu^{(2)} = \mu^{(1)} = \mu$ and thus obtain the simplified boundary integral where the double-layer term on the capsule surface has disappeared (Pozrikidis 1992):

$$\begin{aligned} b\boldsymbol{v}(\boldsymbol{x}) = {} & \frac{1}{8\pi\mu}\int_M \boldsymbol{J}(\boldsymbol{x}, \boldsymbol{y})\cdot\Delta\boldsymbol{f}(\boldsymbol{y})\mathrm{d}A(\boldsymbol{y}) + \frac{1}{8\pi\mu}\int_{W\cup S} \boldsymbol{J}(\boldsymbol{x}, \boldsymbol{y})\cdot\boldsymbol{f}_b(\boldsymbol{y})\mathrm{d}A(\boldsymbol{y}) \\ & - \int_S \boldsymbol{v}^{\infty}(\boldsymbol{y})\cdot\boldsymbol{K}(\boldsymbol{x}, \boldsymbol{y})\cdot\boldsymbol{n}(\boldsymbol{y})\mathrm{d}A(\boldsymbol{y}), \end{aligned} \tag{2.20}$$

where $\boldsymbol{f}_b(\boldsymbol{y})$ represents the force exerted by the boundaries W and S on the suspending liquid and where parameter b takes values $1, 0, 1/2$ when $\boldsymbol{x}$ is located on M, W, S, respectively. The single- and double-layer kernels $\boldsymbol{J}$ and $\boldsymbol{K}$ are defined by

$$J_{ij} = \frac{\delta_{ij}}{|\boldsymbol{x} - \boldsymbol{y}|} + \frac{(x_i - y_i)(x_j - y_j)}{|\boldsymbol{x} - \boldsymbol{y}|^3}, \quad K_{ijk} = -\frac{3}{4\pi}\frac{(x_i - y_i)(x_j - y_j)(x_k - y_k)}{|\boldsymbol{x} - \boldsymbol{y}|^5}. \tag{2.21}$$

Integral (2.20) is further simplified by performing the integration analytically in the azimuth direction. The surface integrals are then reduced to line integrals taken along the intersection curves of surfaces M, W, S with a meridian plane.

2.4. *Main problem parameters*

A dimensional analysis of the problem shows that the main parameters for the flow and capsule properties are:

an equivalent capillary number that measures the ratio of viscous to elastic forces $\varepsilon = \mu Q/\pi R^2 G_s$;

the size ratio between the capsule and the tube a/R (note that the pre-inflated capsule radius is used);

the pre-stress measured by the pre-inflation ratio α;

the ratio of area dilation to shear moduli K_s/G_s;

the ratio of bending to shear moduli $B = B_s/G_s R^2$.

In the following, we consider values of $a/R \in [0.8, 1.0]$, corresponding to medium to large capsules. The maximum capillary number is taken to be 0.6, a fairly large value that is not easy to obtain experimentally. The pre-inflation ratio is at most 10%, corresponding to quite high pre-swelling. Finally, as will be explained later, the ratio B is taken as small as possible to prevent buckling without altering significantly the deformed profile of the capsule.

3. Numerical procedure

We use the numerical procedure initially proposed by Quéguiner & Barthès-Biesel (1997) and later improved by Diaz & Barthès-Biesel (2002) through the use of efficient interpolation techniques to describe the geometry of the deforming boundaries. It consists of following the motion of the capsule as it enters the pore and in tracking the Lagrangian position of the membrane material points. The fluid domain boundaries are tessellated into elements with collocation points, and interpolated by means of cubic B-spline functions. At a given time t, the position of the membrane collocation points is thus known. By comparing the deformed and initial positions, the principal extension ratios, curvatures, bending moments and elastic tensions are computed from (2.7), (2.8), (2.14) and one of the constitutive laws (2.9), (2.10) or (2.12). The load on the membrane surface follows from (2.15) and (2.16). The force distribution $\boldsymbol{f}_b$ on W and the additional pressure drop Δp on S are obtained from boundary conditions (2.4) and (2.19) associated with the boundary integral (2.20) with $\boldsymbol{x}$ located alternately on W and on S, respectively. The capsule membrane velocity is obtained from (2.20) with $\boldsymbol{x}$ located on M. The position of the membrane material points is then updated by means of (2.5).

Our objective is to obtain a steady deformation of the capsule inside the tube. However, achieving this steady state may sometimes require fairly long times or equivalently fairly long tube lengths. In order to limit the dimensions of the flow domain, we switch to a reference system linked to the capsule and moving with it when the particle is well inside the tube with a minimum axial coordinate larger than $4R$. This is possible because the flow disturbance created by the particle is $O(|\boldsymbol{x} - \boldsymbol{x}^{(M)}|^{-2})$. More specifically, Quéguiner & Barthès-Biesel (1997) have shown that Poiseuille flow profiles were recovered within 1% at distances from the front and rear of the capsule of order R. We consider that steady state is reached when $|\partial T_{1max}/\partial t| < 10^{-2} G_s Q/\pi R^3$ and $|\partial \Delta p/\partial t| < 10^{-2} G_s Q/\pi R^4$ where T_{1max} is the maximum elastic tension in the membrane meridian. The entrance section E is located at $R_E = 30R$ and the exit section S at $L = 15R$. The hyperbolic part is tessellated into 66 elements unequally spaced with increasing density as the hyperbola apex is approached. The tube part and exit section S are tessellated into 189 and 34 equally spaced elements, respectively. The membrane meridian is tessellated into 60 or 120 equally spaced

elements on the initial inflated sphere, depending on the flow strength and resulting deformation.

At time $t=0$, the undeformed and pre-inflated capsule is centred at $x^{(M)}=-4R$ and the flow is started. However, it is also possible to start with a deformed capsule inside the tube and use the reference frame linked to the capsule centre. In this case, the deformed shape is not necessarily in equilibrium with the imposed flow conditions, and we run the programme until the capsule has attained a new equilibrium, if any. The numerical scheme uses an explicit time integration procedure and is thus numerically unstable unless the time step Δt is very small. We found that using $\Delta t = 3.2\times10^{-4}\pi R^3/Q$ ensures numerical stability but leads to fairly long computational times since the entrance process is quite slow. With those numerical parameters Diaz & Barthès-Biesel (2002) show that steady values of pressure drop and capsule velocity can be obtained with a precision of about 0.1%. A further check on the precision of the numerical model can be done by monitoring the capsule volume. We have in general a volume change well under 1% even after 240 000 time steps and that is an indication of the numerical precision of the membrane partition used.

All the results presented here satisfy the steady-state criteria. At steady state, there is a significant viscous pressure drop in the sheared liquid film between the capsule and the wall. Since the internal liquid is motionless, the pressure inside the capsule is uniform. Consequently, from equation (2.16), we can expect the meridian rear curvature C_r (at $r=0$) to always be smaller than the meridian front curvature C_f (at $r=0$). This leads to parachute shapes ($C_r<0$) or to slug shapes ($C_r>0$) with the back blunter than the front.

4. Motion of a capsule with an Sk membrane

As an example, we consider a capsule with a membrane that obeys constitutive law (2.10) with $K_s=3G_s$ (i.e. $C=1$). We study the effect of pre-swelling α, flow strength as measured by ε and size ratio a/R on the capsule steady motion. The effect of C and of different membrane laws will be studied later. As in Lac & Barthès-Biesel (2005), three inflation ratios $\alpha=0\%$, 2.5% and 10% are considered. The value 2.5% corresponds to a moderate pre-inflation whereas 10% is a large pre-inflation that leads to high pre-stress and significant apparent hardening of the membrane.

The deformed profiles have a complex shape that is not easy to quantify. Risso *et al.* (2006) have introduced different parameters that can be measured on experimental profiles: the maximum L_x and minimum L_{fr} axial lengths, the maximum transversal length L_y, the deformed meridian perimeter L_m, the front C_f and rear C_r curvatures on the revolution axis (figure 2). We thus compute these geometrical parameters as functions of the problem parameters $\varepsilon, a/R, \alpha$. These results are useful for the analysis of experimental data, as will be illustrated later.

4.1. *Effect of bending resistance*

When the capsule is not pre-stressed, the membrane is subjected to negative elastic tensions along a meridian, especially when the curvature at the back changes sign. This occurs during the transient stage when the capsule enters the pore. In order to prevent buckling, Diaz & Barthès-Biesel (2002) found it necessary to introduce a small bending resistance of the membrane. The non-dimensional bending modulus B was chosen large enough to prevent buckling and allow the capsule to reach a steady shape. However, it was also taken as small as possible to prevent any significant

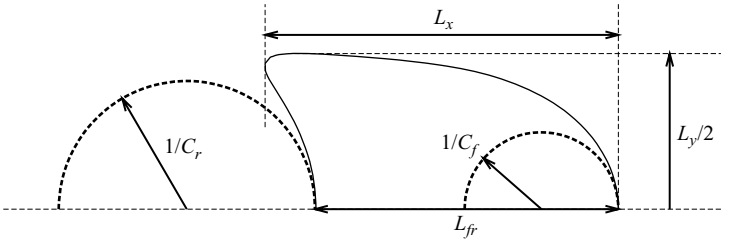

FIGURE 2. Definition of parameters quantifying capsule deformation.

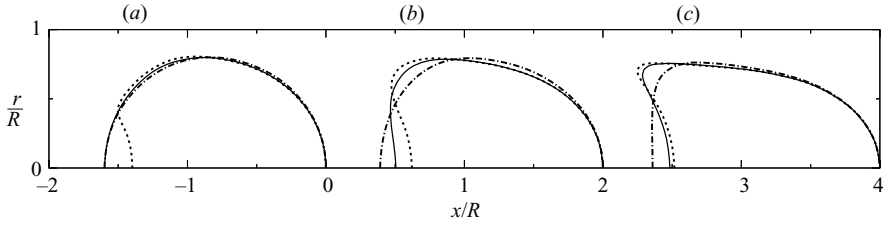

FIGURE 3. Effect of pre-inflation and flow rate on capsule deformed half-profiles ($a/R = 0.8$). (*a*) $\varepsilon = 0.012$, (*b*) $\varepsilon = 0.06$, (*c*) $\varepsilon = 0.24$. Dotted line: $\alpha = 0\%$; continuous line: $\alpha = 2.5\%$; dash-dot line: $\alpha = 10\%$.

modification of the final capsule shape or of the additional pressure drop. Diaz & Barthès-Biesel (2002) found that the value $B = 1 \times 10^{-5}$ served the above purposes for the neo-Hookean membrane they studied.

Owing to its strain-hardening property, an Sk membrane does not buckle for $\alpha = 0$ and flow strengths as large as $\varepsilon = 0.6$, so that a steady shape can be obtained. We find that the profiles computed with $B = 0$ and $B = 1 \times 10^{-5}$ are superimposed within graphical precision, whereas a much larger value $B = 1 \times 10^{-3}$ corresponding to much larger membrane bending resistance, leads to a significantly different capsule shape. When the capsule is pre-inflated, the elastic pre-stress may prevent the appearance of negative tensions in the membrane and thus remove the tendency towards buckling (Lac & Barthès-Biesel 2005). For moderate pre-inflation ($\alpha = 2.5\%$), we find again that the profiles obtained for $B = 0$ and $B = 1 \times 10^{-5}$ superimpose. For large pre-inflation ($\alpha = 10\%$), B has an effect only at very high flow rates but for $\varepsilon = 0.09$ the profiles obtained with $B = 0$, $B = 1 \times 10^{-5}$ and $B = 1 \times 10^{-3}$ superimpose, because the large pre-stress prevents any significant deformation.

It was not our purpose to study the effect of bending rigidity of the membrane, but in order to have a meaningful comparison of $\alpha = 0$ and $\alpha > 0$ results for different membrane constitutive laws, it was decided to use the same small value of ratio of bending to shear moduli $B = 1 \times 10^{-5}$ even for pre-stressed capsules. Occasionally when steady state was reached, the value of B was changed to $B = 0$ and we verified that the new steady deformed profile was not significantly modified.

4.2. *Effect of α and ε ($a/R = 0.8$)*

We now study in detail the combined effects of pre-stress and flow strength for medium-sized capsules such that $a/R = 0.8$. Steady deformed half-profiles are shown in figure 3 as a function of α for three typical values of ε. For small flow strength (e.g. $\varepsilon = 0.012$), the capsule with no pre-stress has a parachute shape with negative rear curvature, whereas a small amount of pre-stress (e.g. $\alpha \geqslant 2.5\%$) prevents the

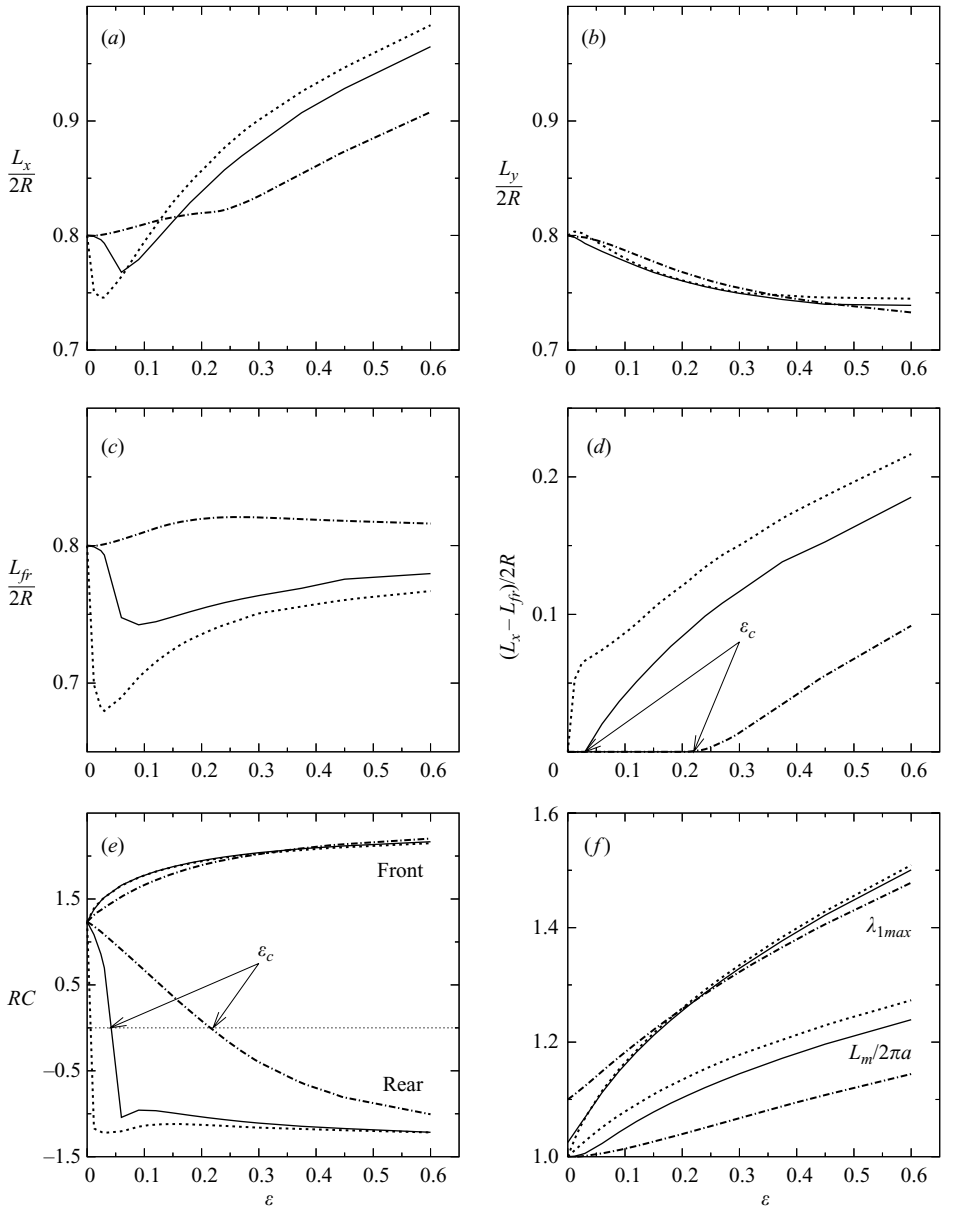

FIGURE 4. Effect of α and ε on the different parameters measuring steady capsule deformation (defined in figure 2), $a/R = 0.8$. In (e), RC represents the non-dimensional curvatures RC_f and RC_r evaluated at the front and the rear respectively. Same legend for α as in figure 3.

curvature inversion. As ε increases to 0.06, the 2.5% pre-inflated capsule exhibits the beginning of a curvature inversion at the rear (figure 3b), whereas for $\alpha = 10\%$, the internal pressure is still large enough to prevent the appearance of the parachute. For high flow strength ($\varepsilon = 0.24$), the difference between pre-stressed ($\alpha = 2.5\%$) and unstressed ($\alpha = 0$) capsules has almost disappeared (figure 3c). The 10% pre-inflated capsule also begins to undergo the curvature inversion at the rear.

In figure 4, we show the variations with ε of $L_x, L_y, L_{fr}, C_f, C_r$ and L_m for the three values of inflation ratio α. We note immediately that the transversal length L_y

a/R	$\alpha = 0\%$	$\alpha = 2.5\%$	$\alpha = 5\%$	$\alpha = 10\%$
0.8	≈ 0	0.043	0.1	0.21
0.9	0.009	0.048	0.096	0.19
1.0	0.02	0.061	0.105	0.19

TABLE 1. Critical values ε_c for which the rear curvature changes sign. The case $\alpha = 5\%$ is added to facilitate interpolation of data.

and the front curvature C_f do not vary much with either ε or pre-stress (figure 4*b*, *e*). It follows that these parameters are not appropriate to evaluate capsule mechanical properties. For moderate or no pre-inflation, the axial length L_x first decreases with ε, while the radial length L_y increases slightly. This corresponds to a small axial compression of the capsule due to the adverse pressure gradient. Then L_x increases continuously with ε, while L_y decreases slightly. When pre-inflation is large ($\alpha = 10\%$), the high internal pressure prevents the initial axial compression of the capsule. Thus L_x is a monotonically increasing function of ε as is apparent in figure 4(*a*). Note though that L_x is measured at different locations as the shape evolves: on the tube axis for slug shapes or on the rim for parachute shapes. As a consequence, for a given value of ε, when α (or equivalently membrane apparent rigidity) increases, L_x either increases ($\varepsilon < 0,06$), decreases and then increases ($0.06 < \varepsilon < 0.15$), or decreases ($\varepsilon > 0.15$). It follows that the measurement of L_x only is not enough to characterize capsule mechanics.

The useful parameters to study the shape evolution from slug to parachute are L_{fr}, the difference $L_x - L_{fr}$ or the rear curvature C_r. As shown in figure 4(*c*), L_{fr} follows the same trend as L_x when ε increases, but becomes smaller than L_x when the parachute is formed. The change in curvature sign at the rear occurs when $L_x - L_{fr}$ becomes positive for a critical value ε_c of capillary number that is fairly sensitive to pre-inflation (figure 4*d*, *e*). Consequently measuring the evolution of $L_x - L_{fr}$ or of C_r with ε may yield the value of ε_c from which pre-inflation can be estimated, as shown in table 1. As ε increases, deformation and thus the capsule meridian perimeter L_m increases (figure 4*f*). However, L_m is not very sensitive to pre-inflation. Indeed for a given ε, varying α from 0 to 10% leads to a global decrease of L_m of order 10%. The value of $L_m/2\pi a$ is equal to the average of the extension ratio λ_1 along a meridian curve. However, the maximum extension ratio in the meridian λ_{1max} is significantly larger than $L_m/2\pi a$ and fairly insensitive to α (figure 4*f*). This is because the maximum extension occurs near the nose of the capsule where the local deformed shape is also insensitive to α as can be seen from the profiles in figure 3 and also from the value of the front curvature in figure 4(*e*). In conclusion, capsule dynamics are defined by the variation with ε and α of two sets of parameters, L_x or L_m, that measure the overall membrane extension, and by $L_x - L_{fr}$ or C_r that measure the parachute depth and lead to an estimate of pre-inflation through ε_c.

4.3. *Effect of capsule size*

It is now of interest to study the combined effects of capsule size and pre-inflation as both phenomena influence the deformed shape of the particle. We thus consider two other size ratios $a/R = 0.9$ and $a/R = 1.0$. Larger values of a/R are usually difficult to achieve experimentally without plugging. The deformed profiles are shown as a function of pre-inflation and flow strength in figures 5 and 6. In the case $a/R = 1.0$ and weak flow ($\varepsilon = 0.012$), all capsules are convex even in the absence of pre-stress

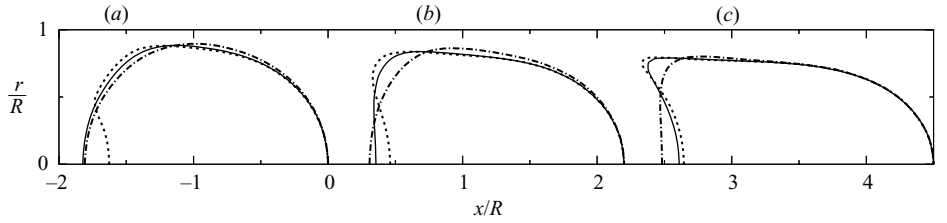

FIGURE 5. Effect of pre-inflation and flow rate on capsule deformation ($a/R = 0.9$). (a) $\varepsilon = 0.012$, (b) $\varepsilon = 0.06$, (c) $\varepsilon = 0.24$. Same legend for α as in figure 3.

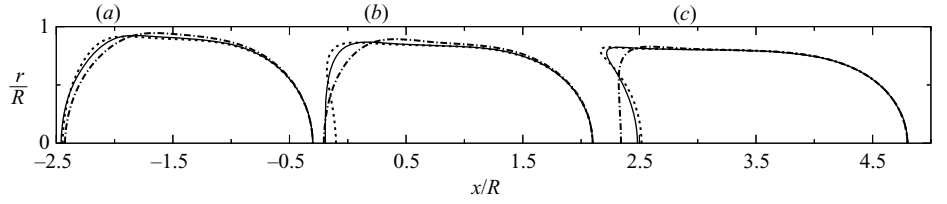

FIGURE 6. As figure 5 but for ($a/R = 1.0$).

(figure 6a). For medium flow ($\varepsilon = 0.06$) and $a/R \geqslant 0.9$, only the capsule with no pre-stress exhibits a concave back (figures 5b and 6b). As we increase ε to 0.24, the 2.5% pre-inflated capsule also takes a parachute shape and its deformed profile becomes very similar to that of the unstressed capsule (figures 5c and 6c). For $\varepsilon = 0.24$, the 10% pre-inflated capsules both have a slightly negative curvature at the back ($C_r \approx -0.2/R$) although it is barely detectable on figures 5(c) and 6(c).

The combined effects of size ratio, pre-inflation and flow strength are summarized in figure 7. For low flow strength, capsules that are smaller than the tube without or with small pre-stress undergo a slight initial axial compression as shown by the initial decrease of $L_x/2R$ and of L_{fr} (figure 7a,b). This initial compression does not occur for large capsules that are constrained by geometry to take a slug shape. As ε increases, L_x seems to increase continuously, while the radial length L_y (not shown) stabilizes to a plateau value that is not very sensitive to either size or pre-inflation. The radial length L_{fr} becomes smaller than L_x when the capsule back becomes concave and then also reaches a plateau value for high flow strength. This phenomenon, coupled with the continuous increase of L_x, shows that the parachute deepens when ε increases as shown by the evolution of $L_x - L_{fr}$ with ε (figure 7c). The deformed perimeter (now scaled with tube radius to show size effects) $L_m/2\pi R$ increases with size and flow strength but decreases with pre-inflation, as expected (figure 7d). In all cases, pre-stress decreases deformation, but its relative effect fades out as ε increases.

The analysis of the effect of size and pre-inflation on the front and rear curvature of the deformed profiles is also interesting. In figure 8, the front curvature C_f is shown only for $\alpha = 2.5\%$ because pre-inflation does not influence C_f much. We find that C_f varies slowly with ε, as pointed out earlier. The front curvature is probably the easiest one to measure, but unfortunately it is not very sensitive to the main flow parameters. The rear curvature C_r however, is sensitive to size ratio and pre-inflation at low capillary numbers except for large pre-inflation ($\alpha = 10\%$) where C_r does not depend much on size for any value of ε (figure 8). For low pre-inflation ($\alpha \leqslant 2.5\%$), the back parachute curvature becomes independent of size for high flow strength ($\varepsilon \geqslant 0.2$).

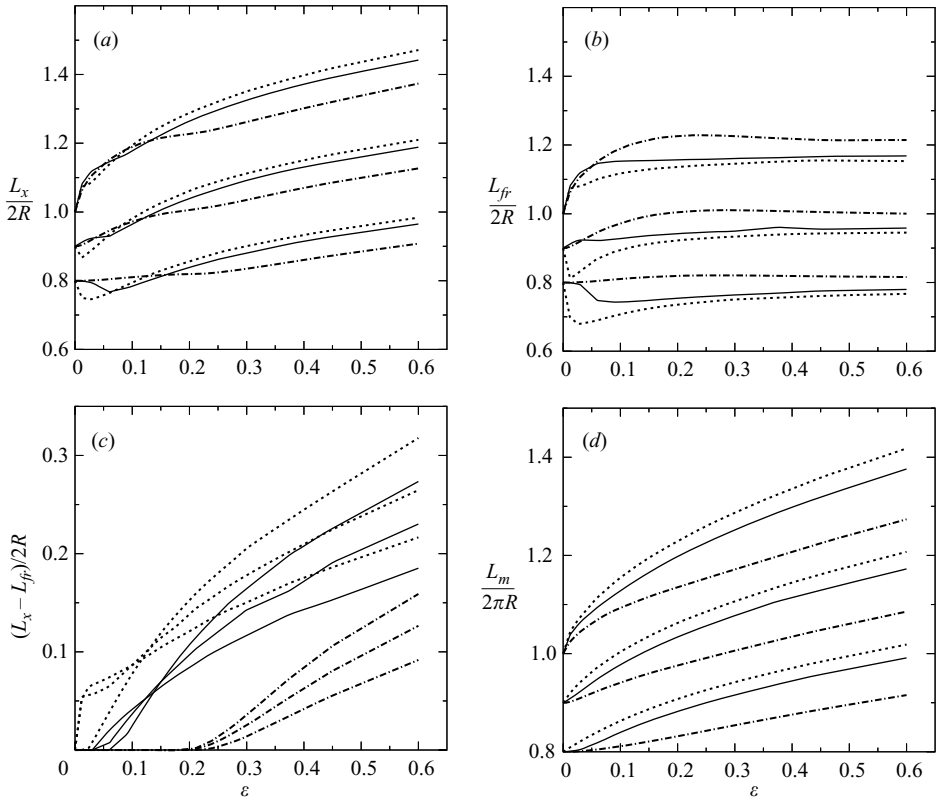

FIGURE 7. Effect of α and ε on the different parameters measuring steady capsule deformation for three size ratios $a/R = 0.8, 0.9, 1.0$. Same legend for α as in figure 3. For $\varepsilon > 0.3$ and a given value of α, the different lengths increase with a/R.

The critical value ε_c of capillary number for which the shape evolves from slug to parachute is determined by the change of sign of C_r or by the first non-zero value of $L_x - L_{fr}$. The value of ε_c is shown in table 1 as a function of size ratio and inflation. It appears that for a given size ratio, ε_c is quite sensitive to pre-inflation. This is an important result for experiment analysis; the data in table 1 can be interpolated and allow the evaluation of the pre-inflation of a capsule of known size from the value of flow rate at which the back curvature changes sign. However, the value of ε_c is fairly independent of capsule size for a given pre-inflation ratio. This results from a complicated nonlinear interplay of pressure drop in the lubrication film and additional internal pressure due to deformation. In figure 9 we compare the deformed profiles at $\varepsilon = 0.06$ and $\alpha = 2.5\%$ of the three capsules $a/R = 0.8, 0.9$ and 1.0 and note that the length of the lubrication film around the capsule increases as a/R increases while the thickness does not change much. The viscous pressure drop between the back and the front of the capsule thus increases with a/R and this promotes the appearance of a negative curvature at the back. However, the deformation of the capsule increases with a/R (as indicated by the values of L_m shown in figure 7*d*). Consequently the elastic tensions and thus the internal pressure also increase and this opposes the formation of the parachute. Since the capsule undergoes large deformations the interplay of the two phenomena is nonlinear and difficult to predict.

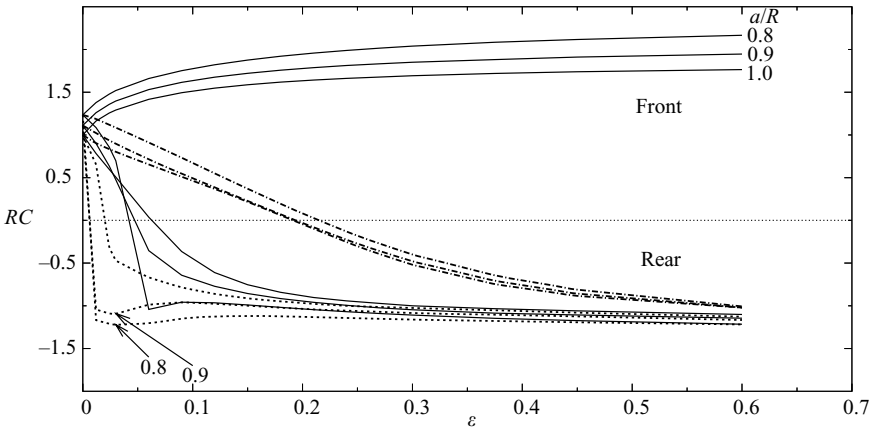

FIGURE 8. Effect of α and ε on the non-dimensional front RC_f and rear RC_r curvatures for three size ratios $a/R = 0.8, 0.9, 1.0$. RC_f is shown only for $\alpha = 2.5\%$. Otherwise, same legend for α as in figure 3

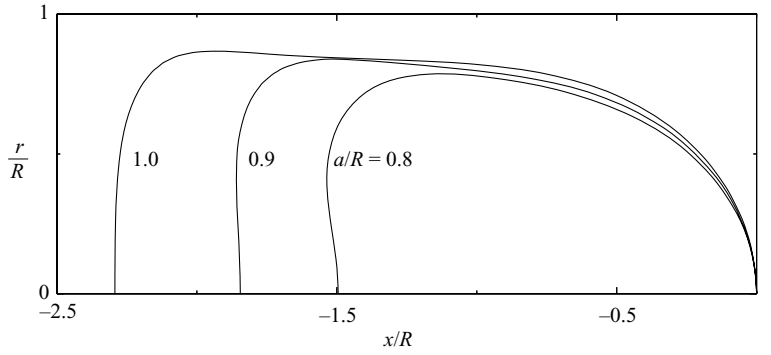

FIGURE 9. Comparison of the deformed profiles at $\varepsilon = 0.06$ and $\alpha = 2.5\%$ for $a/R = 0.8$, 0.9, 1.0. The back curvature is almost the same for the three profiles although their size and deformation differ significantly.

4.4. *Membrane tensions and additional pressure drop*

One of the model's advantages is the evaluation of not measurable quantities such as the elastic tensions in the membrane. The tension T_1 along the meridian is larger than the tension T_2 along parallel curves, except on the tube axis where the two principal tensions are equal. It is of particular interest to determine the maximum of the tension as this information is relevant for break-up. The analysis of tension distribution along a meridian curve shows that T_1 reaches a maximum value slightly before the front tip of the capsule in the upstream part of the lubrication film between the membrane and the wall. The value of the front elastic tension T_{1f} on the axis is a good measure of the overall tension level in the membrane even though it is somewhat smaller (by at most 8%) than the maximum tension in the membrane. The rear tension T_{1r} on the axis is about 10 times smaller than T_{1f}. It first decreases with ε, because the membrane is first compressed before the curvature change occurs. This compression was the main reason why it was found necessary to add a bending resistance to the membrane for $\alpha = 0$. For $\alpha = 2.5\%$, T_{1r} decreases, but remains positive owing to pre-stress. The rear

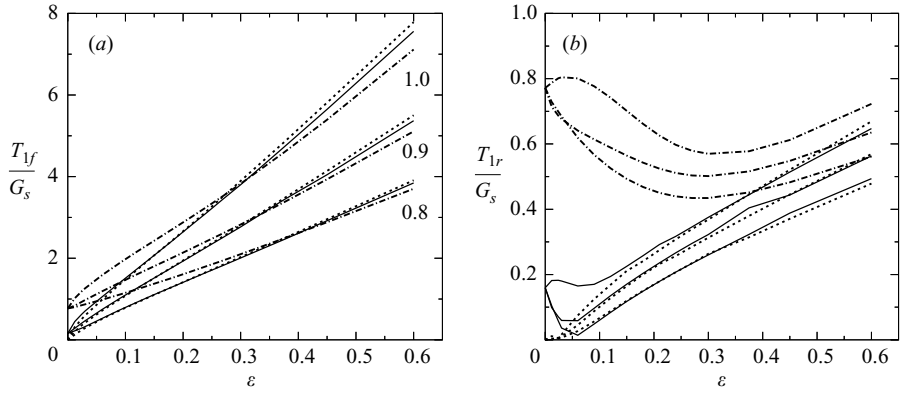

FIGURE 10. Effect of pre-inflation, flow rate and size ratio ($a/R = 0.8, 0.9, 1.0$) on the axial values of tension (a) at the front and (b) at the back. The positive initial value is due to pre-stress. For a given α, the tensions increase with size ratio. Same legend for α as in figure 3.

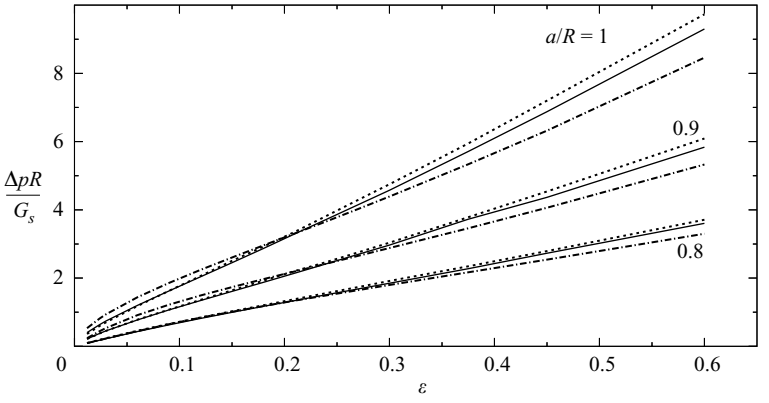

FIGURE 11. Steady additional pressure drop as a function of size ratio, ε and α. Same legend for α as in figure 3.

tension is minimum when the rear curvature C_r is zero. It then increases again as C_r becomes negative, because the parachute is formed and the rear of the capsule is again subjected to stretching forces. We find of course that the minimum of T_{1r} occurs near $\varepsilon = \varepsilon_c$.

The front and rear axial values of the elastic tensions are shown in figure 10 for different values of pre-inflation and all three size ratios. We find that the front tension T_{1f} starts from the initial pre-stress value but no longer depends on this initial pre-stress value for large ε. The front tension increases significantly with size ratio; for $\varepsilon \geqslant 0.3$, T_{1f} is roughy doubled when a/R increases from 0.8 to 1.0. The value of tension at the back is fairly insensitive to pre-stress or size ratio once the parachute is formed ($\varepsilon > 0.4$).

The presence of a capsule in the ube creates an additional pressure drop Δp, that increases with size ratio and flow strength for a given capsule (figure 11). The influence of α is mild at any flow strength, but the influence of size is quite strong since as a/R increases by 25% from 0.8 to 1.0, the additional pressure drop is roughly doubled for any ε. The pressure drop occurs mainly in the viscous film that surrounds

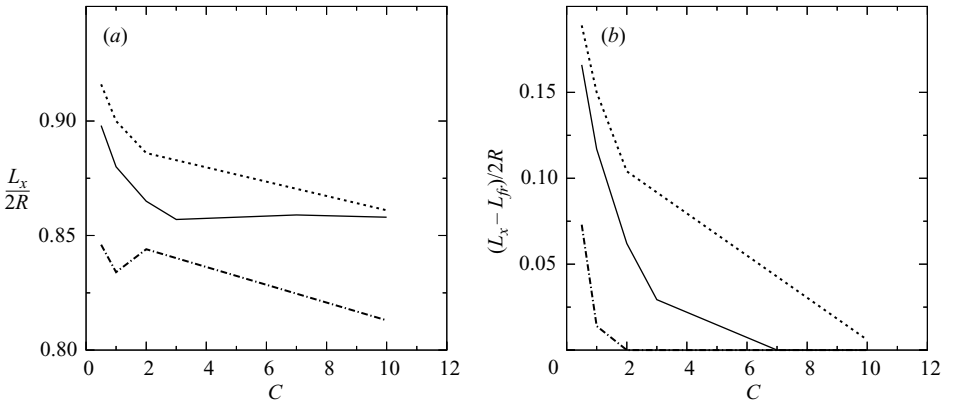

FIGURE 12. Effect of the capsule resistance to area dilation as measured by C for $\varepsilon = 0.3$, $a/R = 0.8$. Same legend for α as in figure 3.

the capsule. The length L_x of this film increases with ε, while the width L_y remains almost constant. Thus the evolution of Δp with ε follows that of L_x.

4.5. *Effect of the ratio K_s/G_s of area dilation to shear in the membrane law*

We now study the effect of the value of parameter C in the membrane law (2.10). The ratio of area dilation to shear modulus K_s/G_s is directly related to C as shown in equation (2.11). When C increases, for a fixed value of ε (equivalently of G_s) the membrane resistance to compression increases and its deformability decreases. As an illustration, we present results for $a/R = 0.8$ and for $\varepsilon = 0.3$, because the influence of C is mainly for large membrane deformation. The effect of C and α on the capsule length L_x and on the depth of the parachute $L_x - L_{fr}$ is shown in figure 12. The global effect of increasing C or K_s/G_s is to decrease the capsule extension and the depth of the parachute. The local increase of L_x that occurs for $\alpha = 2.5\%$ and 10% is due to the change of shape from slug to parachute, as was already noted in § 4.2. We observe also that this shape transition occurs for larger values of C as α decreases (figure 12*b*). We may thus deduce that $\varepsilon_c = 0.3$ for the three sets of parameter values ($\alpha = 0\%$; $C \approx 10$), ($\alpha = 2.5\%$; $C \approx 7$) or ($\alpha = 10\%$; $C \approx 2$).

This short study proves that the area dilation to shear modulus ratio is also an important parameter that influences capsule deformation. The numerical model gives the elastic tension distribution in the membrane. We find that the principal deformation mode is indeed area dilation in the front and rear parts of the capsule, but that shear and area dilation deformations are of the same order of magnitude in the membrane part located in the film region near the wall.

5. Comparison with experimental results

Risso *et al.* (2006) studied experimentally the motion and deformation of capsules flowing in a cylindrical tube. The flow rate Q was imposed by infusion syringe pumps. The capsules were nearly spherical and their radius was measured by means of a video camera. For some reference capsules, the membrane area dilation modulus K_s was determined by means of compression experiments, assuming area dilation was the principal deformation mode. When such a direct evaluation of K_s was not available, an estimate was obtained by comparing the deformed profile to that of a reference capsule with the same size and assuming that the same deformation was obtained for

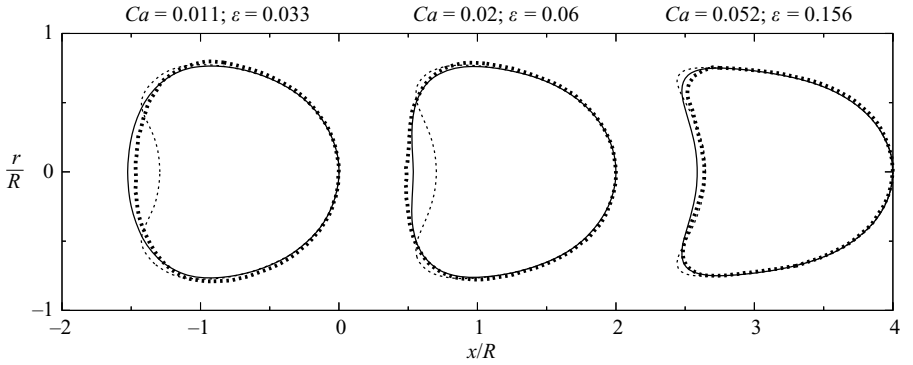

FIGURE 13. Comparison between experimental and numerical deformed profiles for $a/R = 0.77$. Thin dotted line: $\alpha = 0$, continuous line: $\alpha = 3\%$, thick dotted line: experimental profile of Risso *et al.* (2006).

the same value of capillary number. For a given flow rate, Risso *et al.* (2006) could thus compute a capillary number $Ca = \varepsilon G_s/K_s$, defined by an expression similar to that for ε where G_s was replaced by K_s. They also found that the ratio K_s/G_s lay between 1 and 3, but that the exact value had no influence on the results. When the back of the capsule was concave, owing to the formation of the parachute shape, the projection of the parachute edge was deleted manually from the picture, so that the resulting digitalized profiles approach the shape of a meridian curve of the deformed capsule. Thus, for representative capsules, they recorded the deformed profile and measured the lengths L_x, L_y, L_{fr}, L_m and the curvatures C_f and C_r as functions of capillary number. The digitalized experimental profiles of figure 7 in Risso *et al.* (2006) were kindly provided to us by F. Risso. From each deformed profile of a given experimental capsule, we calculate the volume and use the mean of the calculated volumes to determine the radius a of the initial spherical capsule. With this procedure, we find slightly larger values of a than the ones given by Risso *et al.* (2006).

In principle, the deformed shape of the capsule depends on many parameters: membrane constitutive law and K_s/G_s, size ratio a/R, pre-inflation α and flow strength measured by either Ca or ε. It is thus difficult to determine a unique set of values for these parameters that will characterize the capsule. We thus first try to match the experimental data with numerical profiles computed for a capsule enclosed by an Sk membrane with $C = 1$, and then explore other values of C and other membrane constitutive laws.

5.1. *Comparison with a capsule enclosed by an Sk membrane ($C = 1$, $K_s/G_s = 3$)*

The experimental results are now compared to the numerical results presented in § 4 for a capsule with a membrane obeying the Sk constitutive law (2.10) with $C = 1$, thus $K_s/G_s = 3$ and $Ca = \varepsilon/3$.

In figures 13 and 14, we show experimental deformed profiles for size ratios $a/R = 0.77$ and 0.83 ($a/R = 0.75$ and 0.81, respectively in Risso *et al.* 2006), corresponding to capsules that are smaller than the tube and can thus easily flow and deform. Three values of capillary number are considered in each case, for small, medium and high experimental flow strengths. We note that the curvature inversion at the rear of the experimental capsules occurs for values of capillary number larger than $\varepsilon = 0.06$, but probably not much larger since the curvature is already very small

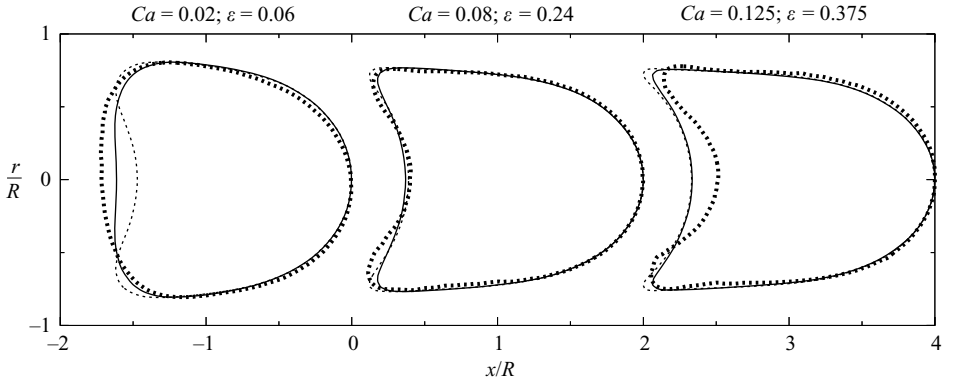

FIGURE 14. As figure 13 but for $a/R = 0.83$.

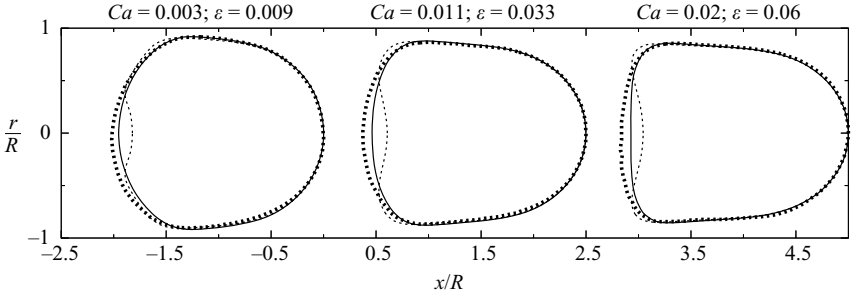

FIGURE 15. As figure 13 but for $a/R = 0.95$.

for $\varepsilon = 0.06$. We then interpolate the results given in table 1 for $a/R = 0.8$ and find $\alpha \approx 3\%$.

Numerical profiles were then computed for the same values of a/R and ε, with $\alpha = 0\%$ (no pre-stress) and $\alpha = 3\%$. We note that for small capillary numbers, the numerical profile with no pre-stress has a concave back whereas the experimental profile is convex (figures 13 and 14). However, when a pre-stress corresponding to $\alpha = 3\%$ is included in the numerical model, the fit between the experimental and numerical profiles is much better, as can be seen in figures 13 and 14. For $a/R = 0.83$ at very large flow strength ($\varepsilon = 0.375$), the back curvature of the experimental profile is larger than the one predicted numerically. The deformed profiles of a large capsule ($a/R = 0.95$, corresponding to $a/R = 0.94$ in Risso *et al.* 2006) are shown in figure 15. The capillary number is not high enough to create a parachute profile but an initially unstressed capsule exhibits a curvature inversion at the back even at these low values of ε. We select the same value $\alpha = 3\%$ as for the smaller capsules and find that there is a very good fit between the numerical pre-inflated profiles and the experimental ones (figure 15).

In view of this profile comparison, we may deduce that the experimental capsules were probably subjected to an initial pre-stress due to osmotic effects caused by partial dissolution of the membrane material during storage. This possibility was also considered by Risso *et al.* (2006), who estimated that the initial pre-inflation was of order 4.5%. Risso *et al.* (2006) also conducted some experiments on capsules that had been specifically pre-inflated by immersion in suspensions with different salt concentrations. Estimating the initial pre-inflation ratio to be 2.5%, 4.5% and

7.5%, they subjected capsules with size $a/R = 0.75$ to increasing flow strengths up to $\varepsilon = 0.09$. They did not find any significant influence of α on either the front or back curvature of the capsules. However, this is not surprising because for such low flow strength, the front curvature does not depend on α as can be surmized from figure 4*e*. Furthermore, for $\varepsilon \leqslant 0.09$, the back of the capsule has either a positive or slightly negative curvature (see figure 3). Since it is in fact the projection of the capsule that is observed experimentally, a slightly hollow back will be hidden by the edge of the parachute and will be difficult to detect. It is only when the parachute is well formed with $C_r = -(0.25 \sim 0.5)/R$ that the parachute can be detected without ambiguity. Here, we find that for the Sk law and $C = 1$, a pre-inflation of order $\alpha = 3\%$ is enough to correlate the experimental profiles for different capillary numbers and size ratios. If we were to use a larger value of α, the absolute value of the back curvature would decrease accordingly (figure 8), and thus the fit with the experimental profile would worsen.

For $a/R = 0.83$ and high flow strength ($\varepsilon = 0.375$) there is a discrepancy between experimental and numerical profiles that cannot be attributed to experimental uncertainty but might be due to plastic deformation or to other nonlinear elastic phenomena not accounted for in the simple numerical model we use. It should be noted that the corresponding experimental capsule had the lowest value of K_s and had been stored in saline solution for over 10 months. Such long storage results in an alteration of the molecular structure of the membrane and a significant decrease of the membrane area dilation modulus compared to capsules freshly prepared (Risso & Carin 2004).

5.2. *Effect of membrane constitutive law ($K_s/G_s = 3$)*

So far, we have compared the experimental results to those computed for a capsule with a membrane obeying the Sk law with $C = 1$. The question that arises now is whether other membrane constitutive laws (such as (2.9) or (2.12)) would fit the experimental results equally well, or better.

As an example, we consider the case $a/R = 0.83$ (the only one for which highly deformed shapes were obtained), assume a pre-inflation $\alpha = 3\%$, and compare the profiles of capsules enclosed by membranes obeying either one of the laws MR ($\Psi = 1$ or 0), Sk ($C = 1$) and ES ($A = 3$), that all correspond to the same small deformation behaviour with $K_s = 3G_s$ ($Ca = \varepsilon/3$). As was noted by Quéguiner & Barthès-Biesel (1997) and by Diaz & Barthès-Biesel (2002), a capsule with a neo-Hookean membrane (i.e. MR with $\Psi = 1$) undergoes continuous elongation and does not reach a steady state when the capillary number exceeds a critical value. Here, even with a 3% pre-inflation, we observe the same phenomenon for a capsule with a neo-Hookean membrane and for flow strengths $\varepsilon \geqslant 0.24$. We can thus conclude immediately that a neo-Hookean constitutive law is not appropriate to model the behaviour of the alginate membrane and thus confirm the conclusions of the compression experiments (Carin *et al.* 2003; Risso & Carin 2004; Rachik *et al.* 2006). However, steady deformed shapes could be obtained with the extreme MR law corresponding to $\Psi = 0$.

The steady numerical deformed profiles are compared with the experimental ones in figure 16(a, b) for two values of capillary number ($Ca = 0.08, \varepsilon = 0.24$) and ($Ca = 0.125, \varepsilon = 0.375$). It appears clearly that the Sk law gives a much better fit of the numerical profile than the MR ($\Psi = 0$) or ES laws. These last two laws predict a larger deformation than is actually observed: the overall extension L_x or the axial length L_{fr} are both over-estimated. This is probably due to the strain-softening properties of the MR and ES laws compared to the strain-hardening feature of the

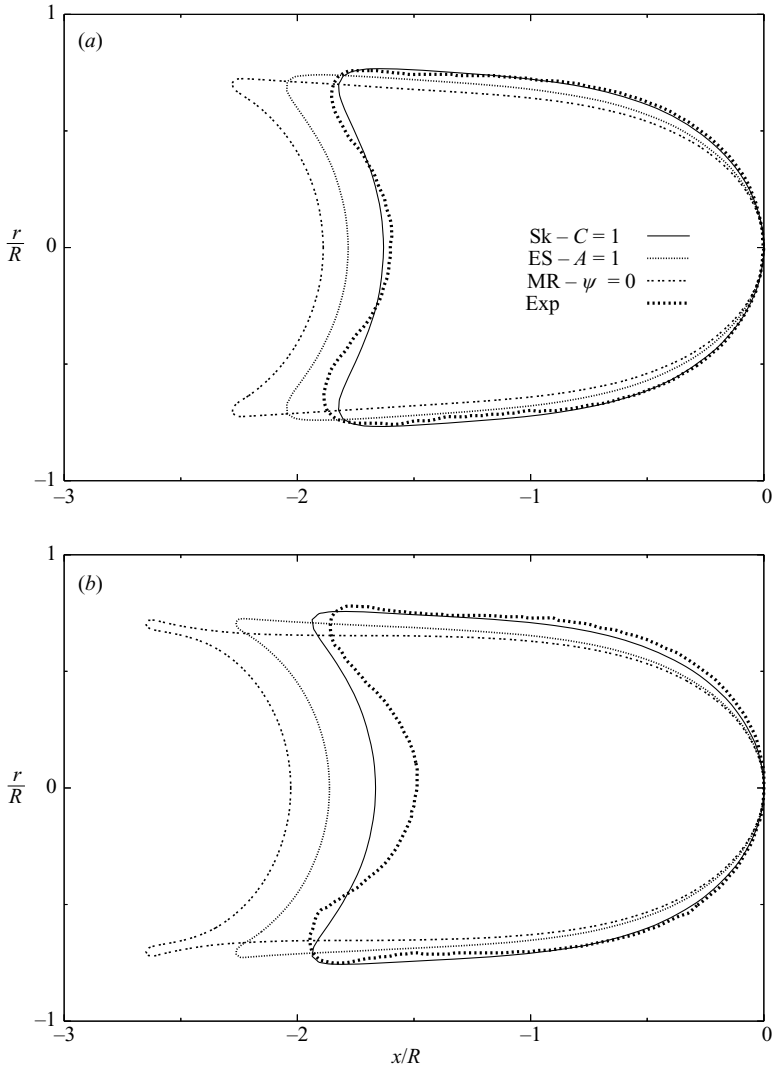

FIGURE 16. Effect of membrane constitutive law on capsule deformed profile for $a/R = 0.83$, $\alpha = 3\%$ and $K_s/G_s = 3$. (*a*) $Ca = 0.08$, $\varepsilon = 0.24$. (*b*) $Ca = 0.125$, $\varepsilon = 0.375$.

Sk law. The discrepancy between the MR or ES profiles and the experimental ones increases with capillary number. Unless we were to use unrealistically large values of α, increasing pre-inflation would not change these conclusions significantly because we are in the large deformation range where the pre-stress influence has faded out.

5.3. *Effect of membrane law parameters*

We now study the effect of the value of the material coefficients in the constitutive laws. Changing C or A modifies the value of the ratio of area dilation to shear modulus K_s/G_s. We consider again the case $a/R = 0.83$ and keep the same value $\alpha = 3\%$. We take the experimental value of Ca as given and compute the corresponding value of ε, using the definition of K_s/G_s given in (2.11) and (2.13). Recall that Risso *et al.* (2006) estimated the ratio K_s/G_s between 1 and 3, corresponding to $C \in [0, 1]$ and $A \in [1, 3]$.

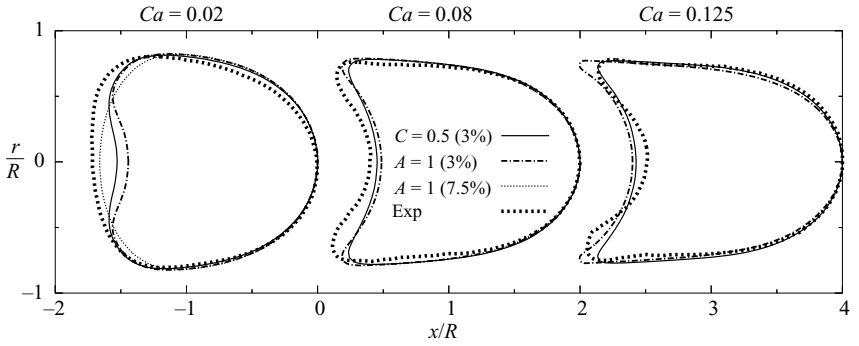

FIGURE 17. Effect of the parameters of the Sk or ES membrane constitutive law on capsule deformed profile for $a/R = 0.83$, $\alpha = 3\%$ or 7.5%.

When we decrease C from 1, we decrease the strain-hardening feature of the Sk law but also the shear capillary number ε. It follows that the profiles obtained for $C = 0$ (not shown) are not deformed enough, while those obtained for $C = 0.5$ slightly underestimate the experimental deformation for $Ca = 0.08$ but give a fair fit for $Ca = 0.125$, as shown in figure 17. In the case of an ES membrane law with $A = 1$, the deformation is also slightly underestimated for $Ca = 0.08$ with values of L_x and L_{fr} smaller than the experimental ones. The profile obtained for $Ca = 0.125$ overestimates L_x and exhibits high curvature on the parachute rim that is not very realistic compared to the experimental profiles (figure 17). Furthermore, for small flow strength $Ca = 0.02$, the experimental profile has a convex back, whereas the numerical profiles both have concave backs with a deeper parachute for ES ($A = 1$) than for Sk ($C = 0.5$). It seems then that these two laws do not fit well the experimental data at low Ca, unless of course we increase pre-inflation. For example for $Ca = 0.02$, a value $\alpha = 7.5\%$ leads to a convex back for the capsule with an ES ($A = 1$) membrane. But as shown in figure 17, the computed deformed shape does not fit well the experimental one for $Ca = 0.02$. Besides, such a high value of α may not be very realistic as the capsules were stored in a supposedly isotonic medium and any pre-inflation, being due to partial membrane dissolution, should remain moderate.

Finally, we may wonder if increasing K_s/G_s would improve the fit between numerical and experimental results. It turns out that this is not the case; for an Sk membrane with $C = 2$ (thus $\varepsilon = 5Ca$), we find that for a set value of Ca, L_x, L_{fr} and C_r all increase with C, corresponding to more elongated profiles with less back concavity.

By looking at the profile comparison in figure 17, one could conclude that if the pre-inflation is kept at the 3% level, then only the Sk ($C = 0.5$) law gives a reasonable fit with the experimental results over the whole range of flow strength. In order to confirm this conclusion, we must validate it for another size ratio. When we consider the case $a/R = 0.95$ for the largest available value of Ca, and compare the experimental profile with those computed for these two laws in figure 18, we note again that the ES law leads to parachute shapes that are not realistic.

From the comparison between the numerical and experimental profiles of flowing capsules, we can draw some conclusions:

(i) the capsule membrane is not well represented by an MR law for any value of the parameter Ψ;

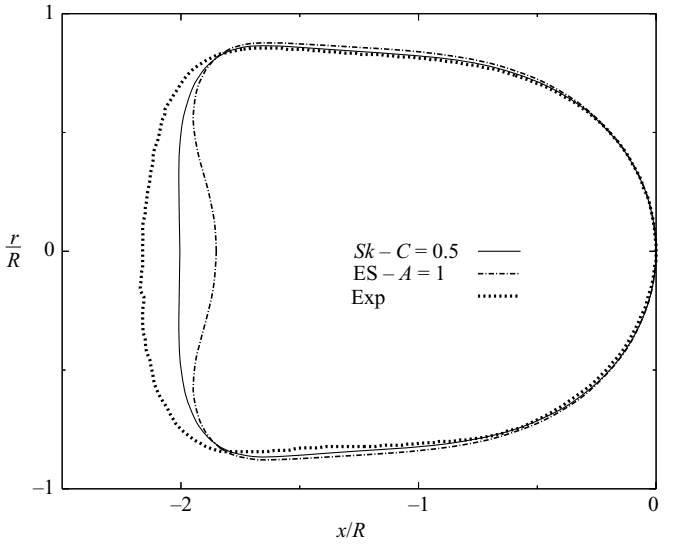

FIGURE 18. Effect of the parameters of the Sk or ES membrane constitutive law on capsule deformed profile for $a/R = 0.95$, $\alpha = 3\%$ and $Ca = 0.02$.

(ii) an ES constitutive law with $A = 3 \sim 1$ does not reproduce well the experimental data for any flow strength and for two size ratios, when the pre-inflation is 3%;

(iii) an Sk constitutive law with C somewhere between 1 and 0.5 and a 3% pre-inflation gives a good fit with the data for all three capsule sizes and all flow strengths.

This result is useful, because it confirms that one single measurement (e.g. compression between two plates) is not enough to determine the constitutive behaviour of the elastic membrane. The MR or ES laws that could be used to analyse the compression data cannot fit the tube flow data well because the deformation and stress fields are different in the two cases. The membrane of the experimental capsules was made of alginate covalently linked to a network of human serum albumin. It is quite possible that under high strain, the albumin network resists deformation and confers strain-hardening properties on the membrane. The fact that the Sk law fits the experimental profiles is probably due to its capacity to reproduce this strain-hardening feature.

6. Conclusion

The flow of a capsule in a cylindrical pore results from a complicated fluid–structure coupling. The geometrical restrictions imposed by the tube wall lead to large deformations that are controlled by the membrane constitutive law. Correspondingly, strain-hardening or strain-softening laws eventually produce very different capsule shapes for a given flow strength. If the membrane elasticity can be evaluated by means of an independent technique (e.g. compression), the value of K_s or G_s is known and the capillary number can be measured. The model then in principle allows a determination, from profile analysis, of possible constitutive laws for the membrane as well as an associated inflation ratio α. Note though, that the analysis of any other independent technique is also constitutive-law dependent if it involves large deformation. Here, for the capsules with a thin alginate membrane studied by Risso

et al. (2006), we find that an Sk law with $K_s/G_s = 3$–2 can approximately represent the experimental data, provided a pre-swelling of 3% is accounted for.

In many situations, it is only possible to obtain one measurement of capsule deformability. Such is the case for very small capsules with micron-size diameters for which compression experiments are very difficult to perform. However, it is feasible to flow a micro-capsule suspension in a capillary tube, where the particle relative size, deformation and velocity can be measured. The easiest way to analyse the data is then first to assume a membrane constitutive law with a given value of K_s/G_s (the choice of law can be guided by the membrane physio-chemical properties). The geometry of the deformed capsule (e.g. L_x, L_{fr}) leads to a value of capillary number from which G_s can be inferred. Then, the eventual pre-inflation may be determined by monitoring the rear curvature change of a flowing capsule and measuring the value of capillary number ε_c for which it occurs. For a given size ratio a/R and membrane law, ε_c depends on pre-inflation as indicated in table 1. The validity of the choice of the constitutive law can be tested with different size capsules and different flow strengths. The constitutive law may not be unique, but can usefully allow the determination of some capsule mechanical properties for comparison purposes. Other effects can also be studied with this model, such as the role of the bending resistance or of other types of laws.

The authors would like to thank Dr Frédéric Risso for providing the experimental profiles of the capsules and for many fruitful discussions. They gratefully acknowledge access to computer resources PILCAD (Plateforme Inter-Laboratoires de CAlcul Distribué) financed in part by ANVAR, HEUDYASIC and ROBERVAL laboratories (Université de Technologie de Compiègne).

REFERENCES

Barthès-Biesel, D. 2003 *Modelling and Simulation of Capsules and Biological Cells*, pp. 1–31. Chapman & Hall/CRC.

Barthès-Biesel, D., Diaz, A. & Dhenin, E. 2002 Effect of constitutive laws for two dimensional membranes on flow-induced capsule deformation. *J. Fluid Mech.* **460**, 211–222.

Carin, M., Barthès-Biesel, D., Edwards-Levy, F., Postel, C. & Andrei, C. D. 2003 Compression of biocompatible liquid filled hsa-alginate capsules: determination of the membrane mechanical properties. *Biotech. Bioengng* **82**, 207.

Diaz, A. & Barthès-Biesel, D. 2002 Entrance of a bioartificial capsule in a pore. *Comput. Model. Engng Sci.* **3** (3), 321–337.

Diaz, A., Pelekasis, N. A. & Barthès-Biesel, D. 2000 Transient response of a capsule subjected to varying flow conditions : effect of internal fluid viscosity and membrane elasticity. *Phys. Fluids* **12**, 948–957.

Eggleton, C. D. & Popel, A. S. 1998 Large deformation of red blood cell ghosts in a simple shear flow. *Phys. Fluids* **10**, 1834–1845.

Evans, E. A. & Skalak, R. 1980 *Mechanics and Thermodynamics of Biomembranes*. CRC.

Kraus, M., Wintz, W., Seifert, U. & Lipowsky, R. 1996 Fluid vesicle in shear flow. *Phys. Rev. Lett.* **77**, 3685–3688.

Kühtreiber, W. M., Lanza, R. P. & Chick, W. L. 1998 *Cell Encapsulation Technology and Therapeutics*. Birkhäuser.

Kwak, S. & Pozrikidis, C. 1998 Adaptive triangulation of evolving, closed or open surfaces by the advancing-front method. *J. Comput. Phys.* **145**, 61–88.

Lac, E. & Barthès-Biesel, D. 2005 Deformation of a capsule in simple shear flow: effect of membrane prestress. *Phys. Fluids* **17**, 0721051–0721058.

Lac, E., Barthès-Biesel, D., Pelekasis, N. A. & Tsamopoulos, J. 2004 Spherical capsules in three-dimensional unbounded stokes flow: effect of the membrane constitutive law and onset of buckling. *J. Fluid Mech.* **516**, 303–334.

Li, X. Z., Barthès-Biesel, D. & Helmy, A. 1988 Large deformations and burst of a capsule freely suspended in an elongational flow. *J. Fluid Mech.* **187**, 179–196.

Pozrikidis, C. 1992 *Boundary Integral and Singularity Methods for Linearized Viscous Flow*. Cambridge University Press.

Pozrikidis, C. 2003*a* Deformed shapes of axisymmetric capsules enclosed by elastic membranes. *J. Engng Maths* **45**, 169–182.

Pozrikidis, C. 2003*b* *Modeling and Simulation of Capsules and Biological Cells*, pp. 35–102. Chapman & Hall/CRC.

Pozrikidis, C. 2005 Axisymmetric motion of a file of red blood cells through capillaries. *Phys. Fluids* **17**, 031503/1–031503/14.

Quéguiner, C. & Barthès-Biesel, D. 1997 Axisymmetric motion of capsules through cylindrical channels. *J. Fluid Mech.* **348**, 349–376.

Rachik, M., Barthès-Biesel, D., Carin, M. & Edwards-Levy, F. 2006 Identification of a bioartificial microcapsule wall material parameter with an inverse method and the compression test. *J. Colloid Interface Sci.* **301**, 217–226.

Ramanujan, S. & Pozrikidis, C. 1998 Deformation of liquid capsules enclosed by elastic membranes in simple shear flow: Large deformations and the effect of capsule viscosity. *J. Fluid Mech.* **361**, 117–143.

Risso, F. & Carin, M. 2004 Compression of a capsule: Mechanical laws of membranes with negligible bending stiffness. *Phys. Rev.* E **69**, 061601–061608.

Risso, F., Collé-Paillot, F. & Zagzoule, M. 2006 Experimental investigation of a bioartificial capsule flowing in a narrow tube. *J. Fluid Mech.* **547**, 149–173.

Secomb, T. W. 1995 Mechanics of blood flow in the microcirculation. *Symp Soc Expl Biol.* **49**, 305–321.

Sherwood, J. D., Risso, F., Collé-Paillot, F., Edwards-Lévy, F. & Lévy, M. C. 2003 Transport rates through a capsule membrane to attain Donnan equilibrium. *J. Colloid Interface Sci.* **263**, 202–212.

Skalak, R., Tozeren, A., Zarda, R. P. & Chien, S. 1973 Strain energy function of red blood cell membranes. *Biophys. J.* **13**, 245–264.